Molecular Therapy
Nucleic Acids
Original Article

Engineered CRISPR-Cas13a system with enhanced target RNA cleavage activity and reduced collateral activity for therapeutic applications

Wenxia Zhang,[1] Haili Wang,[1] Dongzi Liu,[1] Xi Mao,[1] Yi Zhang,[1] Yimu Yang,[1] Zehui Liu,[1] Tong Pan,[1] Yingle Liu,[1,2] and Qi Zhang[1]

[1]State Key Laboratory of Virology and Biosafety, College of Life Sciences, Wuhan University, Wuhan, Hubei 430072, China; [2]Frontier Science Center for Immunology and Metabolism, Wuhan University, Wuhan, Hubei 430072, China

The CRISPR-Cas13 system exhibits potent RNA cleavage activity and has been widely utilized for RNA-targeting applications. However, its collateral cleavage of bystander RNAs limits *in vivo* therapeutic applications. In this study, we generated a series of LwaCas13a mutants through structure-based design and site-directed mutagenesis strategies. A triple mutant enCas13a (Q521R/E796A/E810A) was obtained with significantly enhanced target RNA cleavage activity along with only slightly increased collateral activity. To reduce the collateral activity, we optimized crRNA terminal extensions and obtained M1crRNA and M3crRNA variants that, in combination with enCas13a, maintained or reduced collateral activity while preserving enhanced targeted cleavage activity. Thus, by optimizing the Cas protein and crRNA, we have created an improved CRISPR-Cas13a system with enhanced target RNA cleavage activity and reduced collateral activity. This system demonstrated superior performance in targeting endogenous genes and antiviral applications. Mechanistic studies revealed that enhanced protein-crRNA interactions and altered complex conformations underlie the improved cleavage activity. This engineering approach provides a generalizable strategy for developing CRISPR-Cas systems with enhanced therapeutic potential.

INTRODUCTION

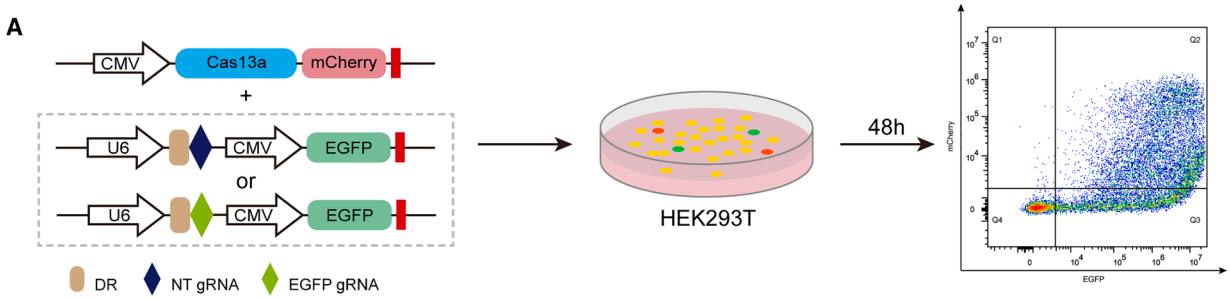
CRISPR (clustered regularly interspaced short palindromic repeat) systems, composed of RNA-guided endonucleases and CRISPR RNA (crRNA), participate in bacterial and archaeal adaptive immunity.[1,2] Currently, the CRISPR-Cas systems can be categorized into two major classes based on the composition of the effector proteins. Class 1 includes types I, III, and IV, and class 2 includes types II, V, and VI.[3,4] Class 2 systems are preferred for biotechnological applications because they are simpler than class 1 systems. Among the class 2 systems, Cas12a (type V) and Cas13a (type VI) exhibit promiscuous DNase and RNase activity upon target recognition to cleave non-target single-stranded DNA and RNA (*trans*-cleavage activity), respectively.[5–7] The Cas13 protein family has been shown to have high efficiency and specificity in programmable RNA targeting and has been widely used for the cleavage and subsequent degradation of RNAs in yeast, plants, flies, zebrafish, mammals, and viruses.[8–15] Cas13 nucleases contain a separate RNase activity that is used to process precursor crRNA into mature crRNA. The conserved higher eukaryotes and prokaryotes nucleotide-binding (HEPN) domains of Cas13 form a composite RNase active center responsible for catalyzing target RNA cleavage. Once the target RNA cleavage activity is activated, the *trans*-cleavage activity of Cas13 nucleases is also activated.[5,8,16] To date, collateral RNA degradation induced by Cas13 has been found in flies, mammalian cells, and mammals.[17–20] Therefore, comprehensive analysis of collateral RNA degradation and its elimination are required for *in vivo* applications of Cas13 systems.

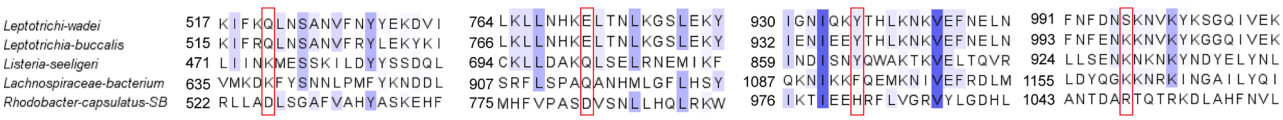
Cas13a, the VI-A subtype of the Cas13 family, has now been employed in RNA editing, nucleic acid detection, viral diagnostics, antiviral therapies, gene regulation, RNA imaging, and biosensing.[12,14,21–26] East et al. first detected the bacteriophage λ gene by harnessing the RNA-guided *trans*-cleavage activity of LbuCas13a.[27] Subsequently, Gootenberg et al. designed the SHERLOCK nucleic acid detector by utilizing the powerful collateral cleavage activity (also known as *trans*-cleavage) of LwaCas13a.[22] In 2018, Gootenberg JS et al. further improved Sherlock's detection limit, specificity, and portability by optimizing nucleic acid amplification, signal amplification, crRNA design, and reagent formulation to make Sherlock more practical.[23] With the good comes the bad; the strong collateral cleavage activity also poses significant challenges for therapeutic use *in vivo*. Many studies have shown that the collateral activity of CRISPR-Cas13a degrades bacterial RNA, which in turn restricts host bacterial growth and leads to bacterial dormancy.[5,28]

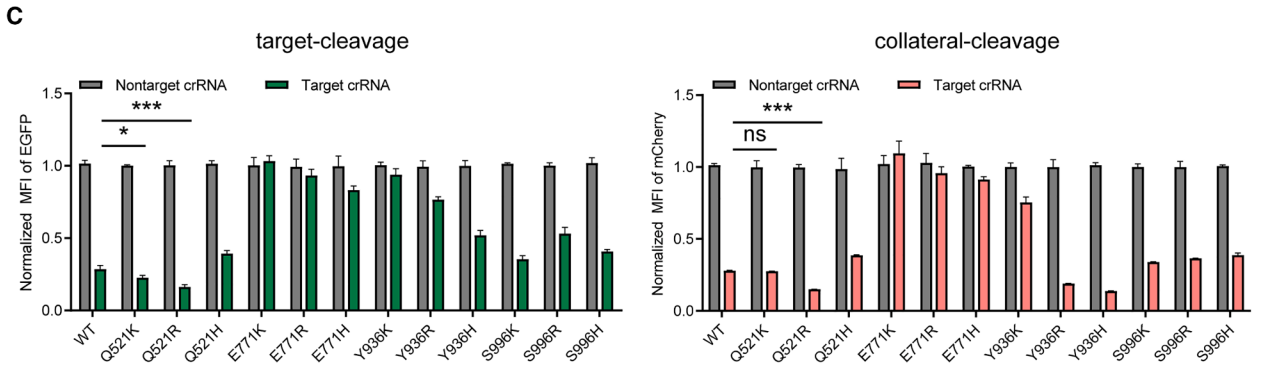
Received 15 July 2025; accepted 22 December 2025;
https://doi.org/10.1016/j.omtn.2025.102811.

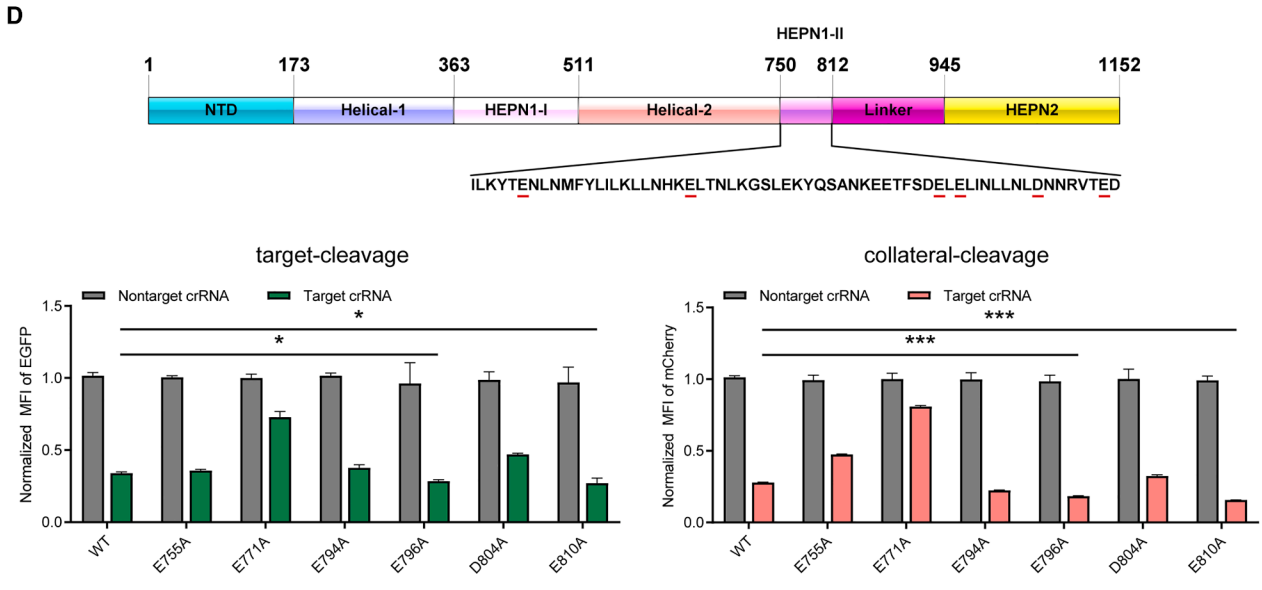
Correspondence: Yingle Liu, State Key Laboratory of Virology and Biosafety, College of Life Sciences, Wuhan University, Wuhan, Hubei, China.
E-mail: mvlwu@whu.edu.cn
Correspondence: Qi Zhang, State Key Laboratory of Virology and Biosafety, College of Life Sciences, Wuhan University, Wuhan, Hubei, China.
E-mail: gracetey@whu.edu.cn

Published by Elsevier Inc. on behalf of The American Society of Gene and Cell Therapy.
This is an open access article under the CC BY-NC-ND license (http://creativecommons.org/licenses/by-nc-nd/4.0/).









(legend on next page)

Methods for optimizing Cas proteins currently include structure-guided engineering, size adjustment of Cas proteins, directed evolution, and integration of nuclease domains.[29–32] Alterations to the crRNA also affect the activity of Cas proteins. Gene editing of the AsCpf1 RNP can be improved by extending the 5' end of the crRNA, whereas TA extension at the 3' end of the LbCas12a crRNA improves the collateral cleavage activity of LbCas12a and FnCas12a.[33,34] Recent studies have shown that adding a U7 extension to the 5' end of crRNA in the 24nt spacer region can enhance the *trans*-cleavage activity of LbuCas13a.[35]

In this study, we constructed a fast and sensitive dual fluorescent reporter system for detecting targeted and collateral cleavage activity. Through structure-based design and site-directed mutagenesis, we generated a series of variants with mutations at the putative protein-crRNA interaction sites and the HEPN1-II domains. We identified a triple mutant (enCas13a: Q521R/E796A/E810A) that improved targeted cleavage with modest collateral increase. To compensate, crRNA variants (M1crRNA and M3crRNA) were designed to suppress collateral activity while retaining or enhancing targeted efficacy. Our results demonstrate that cooperative engineering of both protein and RNA components can yield a more precise and efficient CRISPR-Cas13a system, opening avenues for therapeutic and diagnostic applications.

RESULTS

Engineered LwaCas13a enhances the targeted cleavage efficiency of CRISPR-Cas13a system

To enhance the targeted cleavage activity of LwaCas13a, we aimed to strengthen its interactions with RNA substrates. Protein sequence comparison and homology modeling analysis showed high similarity between LwaCas13a and LbuCas13a (Figures S1A and S1B). Based on this, we hypothesized that key contact sites in the LbuCas13a-crRNA-target complex would also exist in the LwaCas13a-crRNA-target complex.[7] We screened four LbuCas13a residues (Q519, E773, Y938, and K998), whose mutation to alanine impairs cleavage efficiency; these correspond to Q521, E771, Y936, and S996 in LwaCas13a, respectively (Figure 1B). It has been shown that the introduction of basic residues such as lysine (K) or arginine (R) into Cas proteins may increase their affinity to nucleic acids, resulting in boosted cleavage activity.[29,36] We therefore mutated these four residues to generate 12 LwaCas13a mutants. We established a dual fluorescence reporting system to assess the targeted (*cis*-) and collateral (*trans*-) RNA cleavage efficiency of Cas13a. HEK293T cells were co-transfected with Cas13a-mCherry plasmid (encoding Cas13a and mCherry protein) and crRNA-EGFP plasmid (encoding crRNA and EGFP protein). The mCherry signal indicates the expression of Cas13a and its collateral cleavage activity. The crRNA targets the EGFP mRNA, and the EGFP signal indicates the targeting activity of Cas13a. EGFP and mCherry expressions were measured 48 h later by flow cytometry; a decrease in mean fluorescence intensity (MFI) represents the cleavage efficiency of Cas13a (Figure 1A). Fluorescence analysis showed that substitution of Q521 with lysine or arginine significantly increased target RNA cleavage. In contrast, mutation at S996 slightly decreased both targeted and collateral cleavage activities (Figure 1C). Further analysis showed that most regions in the Cas13a active cavity are positively charged.[37] We hypothesized that negatively charged residues in the active cavity might hinder nucleic acid binding, thus affecting the cleavage efficiency. Through studies of the LbuCas13a-crRNA structure and other publications, we have discovered that the HEPN1-II region primarily interacts with the 28-bp guide-target RNA duplex.[7,37] Therefore, excluding the residues in the putative HEPN1-II domain that have already been shown to affect Cas13a cleavage activity through mutation, we screened for several other acidic amino acid residues and mutated them to alanine.[7] It was shown that mutation of residues E796 and E810 to alanine enhanced the cleavage efficiency of Cas13a (Figure 1D).

To obtain a mutant with maximized targeted activity and minimized collateral activity, we combined beneficial single mutations (mutations with high targeted cleavage activity or low collateral cleavage activity) into double (Figure 2A) and triple (Figure 2B) mutants. We found that the double mutants Q521K/E796A, Q521R/E796A, Q521K/E810A, and Q521R/E810A increased the targeted cleavage activity by 14.36%, 13.47%, 12.06%, and 10.12%, respectively, relative to wild-type (WT) Cas13a. However, all these four double mutants showed some increase in collateral cleavage activity (Figure 2A). All triple-mutant results showed a similar pattern. When all effective mutants were pooled, the Q521R/E796A/E810A mutant exhibited the highest targeted cleavage enhancement with the smallest increase in collateral cleavage (Figure 2C). Thus, Q521R/E796A/E810A mutant, hereafter named enhanced Cas13a (enCas13a), was used in subsequent experiments.

crRNA end extensions affect CRISPR-Cas cleavage efficiency

crRNA is an integral part of the CRISPR-Cas system. To further improve the cleavage ability of the CRISPR-Cas system, we also modified the crRNA. First, we tried to optimize the length of the spacer and found that the spacer length should be at least 24 nt to achieve the full activity of CRISPR-Cas13a, which is consistent with previous studies (Figure 3B).[7] We selected a wild-type crRNA (wt crRNA) consisting of a 36 nt direct repeat region and a 28 nt spacer region for crRNA engineering. We predicted the structure

Figure 1. Engineering LwaCas13a to enhance RNA knockdown efficiency

(A) Schematic diagram of the mammalian dual-fluorescence reporter system. (B) Sequence alignment of LwaCas13a and its homologous proteins. Candidate mutagenic regions are marked in the red box. (C) Comparison of the cleavage effect of LwaCas13a mutant and WT in HEK293T cells. The fluorescence intensity level of EGFP represents the targeted cleavage effect of Cas13a (left); the fluorescence intensity level of mCherry represents the collateral cleavage effect of Cas13a (right). (D) Structure-guided mutation and corresponding activity assessment. Mutation candidates in the HEPN1-II domain are marked in red lines. Data were compared using a two-tailed unpaired Mann-Whitney U test. Data are presented as median ± IQR ($n = 4$). $^{*}p < 0.05$; $^{***}p < 0.001$; ns, not significant.

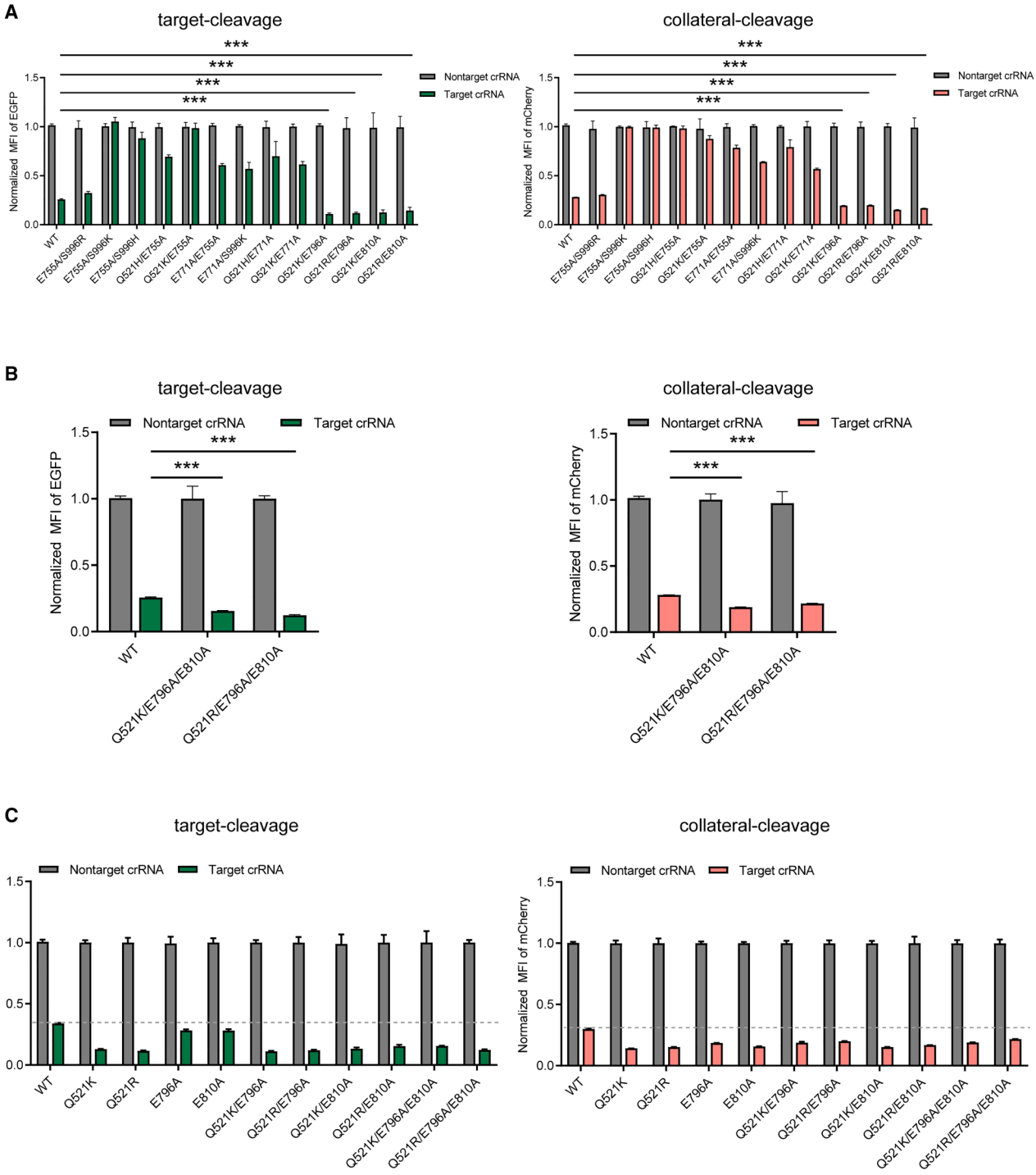
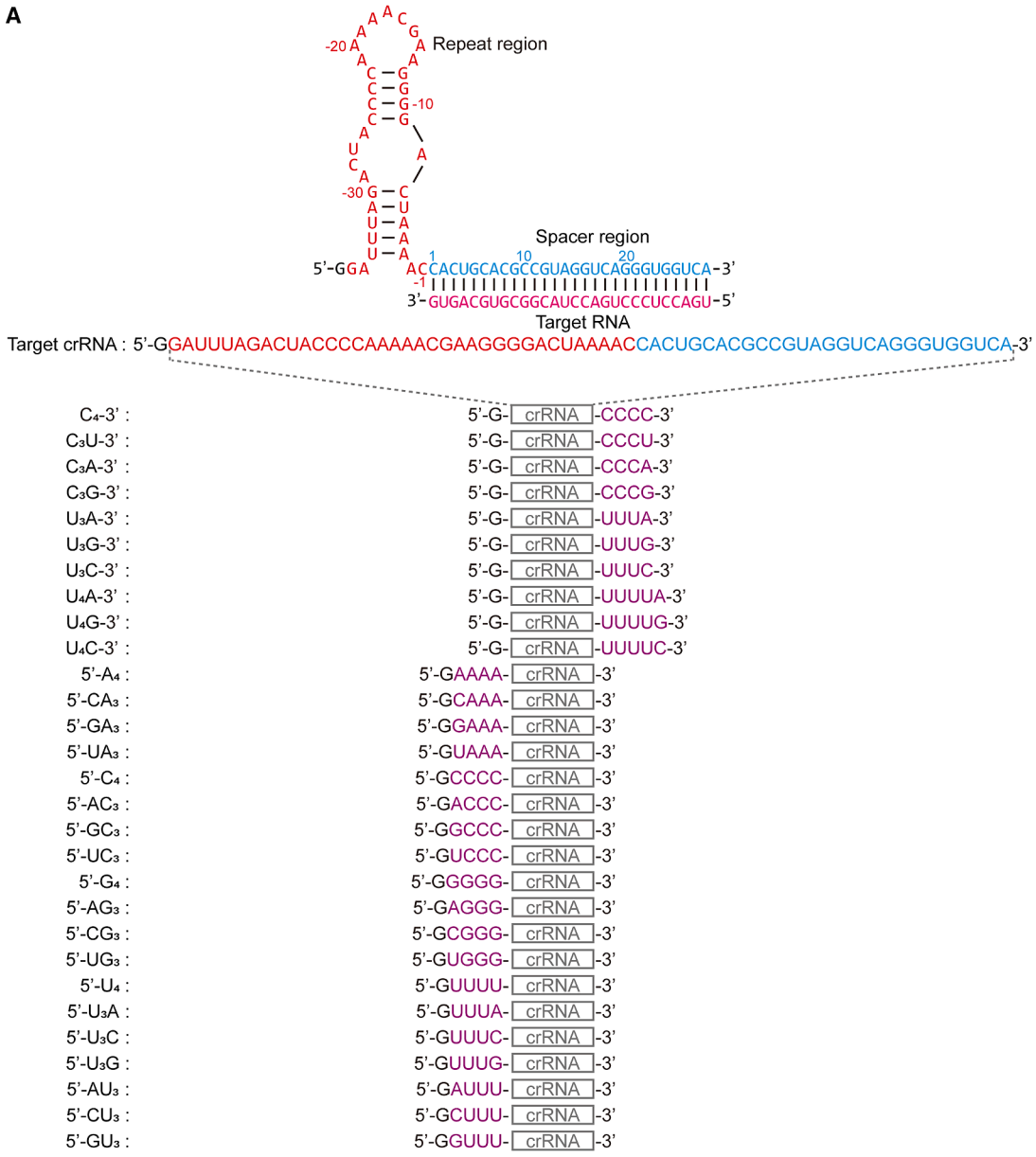


Figure 2. Activity profiling of Cas13a mutations

(A) The targeted (EGFP) and collateral (mCherry) cleavage activities of Cas13a double mutants. (B) The targeted (EGFP) and collateral (mCherry) cleavage activities of Cas13a triple mutants. (C) The targeted (EGFP) and collateral (mCherry) cleavage activities of all the Cas13a beneficial mutants. Data were compared using a two-tailed unpaired Mann-Whitney U test. Data are presented as median ± IQR (n = 4). ***$p < 0.001$.



(legend on next page)

of this crRNA using RNAfold and performed RNA modification based on the structure (Figure 3A).

We modified the 3' end of the crRNA with A_3, G_3, or C_3 extensions and found that the C_3 extension reduced collateral cleavage activity without compromising targeted activity (Figure S2A). We expanded the C_3 extension with an additional base and found that the C_3H (A/U/C) modification further suppressed collateral cleavage activity while improving on-target cleavage activity (Figure 4A). We also modified the 3' end of the crRNA with U_3 or U_4 extensions. Since the transcription of crRNA is regulated by the U6 promoter (recognized by Pol III), to avoid the U_3 or U_4 extensions at the 3' end being recognized as the transcription terminator,[38] we added an extra base A, C, or G after these extensions. Results showed that the U_3A and U_4A extensions exhibiting good cleavage activity, which is consistent with previous studies (Figure 4B).[39] Doubling these extensions at the 3' end of the crRNA, however, did not further increase the cleavage activity (Figure S2B).

We next investigated the 5' end modifications of the crRNA. Among all mutants, U_3A, U_3C, U_3G, and AU_3 (hereafter referred to as M1crRNA) increased targeted cleavage activity by at least 24% with little changes in the collateral cleavage activity (Figure 4C). We then investigated the effects of the combination of 3' and 5' end beneficial modifications and found that the 5'-U_3A plus U_4A-3' (hereafter referred to as M2crRNA) modification significantly enhanced both the targeted cleavage activity and collateral cleavage activity. In contrast, the 5'-U_3C plus C_4-3' (hereafter referred to as M3crRNA) modification enhanced targeted cleavage activity and reduced the collateral cleavage activity (Figure 4D). We compared all the beneficial modifications (the 3', 5', and 3' plus 5' end modifications) and found that the M3crRNA mutants performed best (Figure 4E). Cell viability assays confirmed these findings: M1crRNA and M3crRNA showed minimal cytotoxicity, whereas M2crRNA showed reduced viability (Figure 5). In summary, we finally obtained M3crRNA that met our expectations (high targeted cleavage activity, low collateral cleavage activity) by modifying the ends of the crRNA.

Engineered CRISPR-Cas13a system exhibits superior cleavage activity in mammalian cells

We evaluated the performance of engineered CRISPR-Cas13a system (enCas13a combined with different crRNA mutants) with the dual fluorescence assay. As shown in Figure 6A, enCas13a outperformed wild-type Cas13a in targeted cleavage activity across all crRNA types, while maintaining or reducing the collateral cleavage activity. Comparative analysis with the Cas13X.1 system further demonstrated that enCas13a exhibited superior on-target activity and significantly lower collateral effects (Figure S2C). Given that the dual fluorescent system is exogenous, we next determined the RNA interference efficiency of the engineered CRISPR-Cas13a system on endogenous genes by quantitative PCR (qPCR). We targeted RPL4, RPS5, PPIA, EZH2, EGFR, and PPARG, whose expression levels range from high to low in HEK293T cells, with a single crRNA for each gene.[15] As shown in Figure 6B, all enCas13a groups exhibit at least 10% higher knockdown efficiency compared to Cas13a (WT group) when targeting high-abundance gene RPL4. For low-abundance genes (e.g., EZH2 and PPARG), enCas13a paring with crRNA mutants significantly increased knockdown efficiency. Taken together, these results indicate that the engineered CRISPR-Cas13a system can effectively knock down endogenous genes.

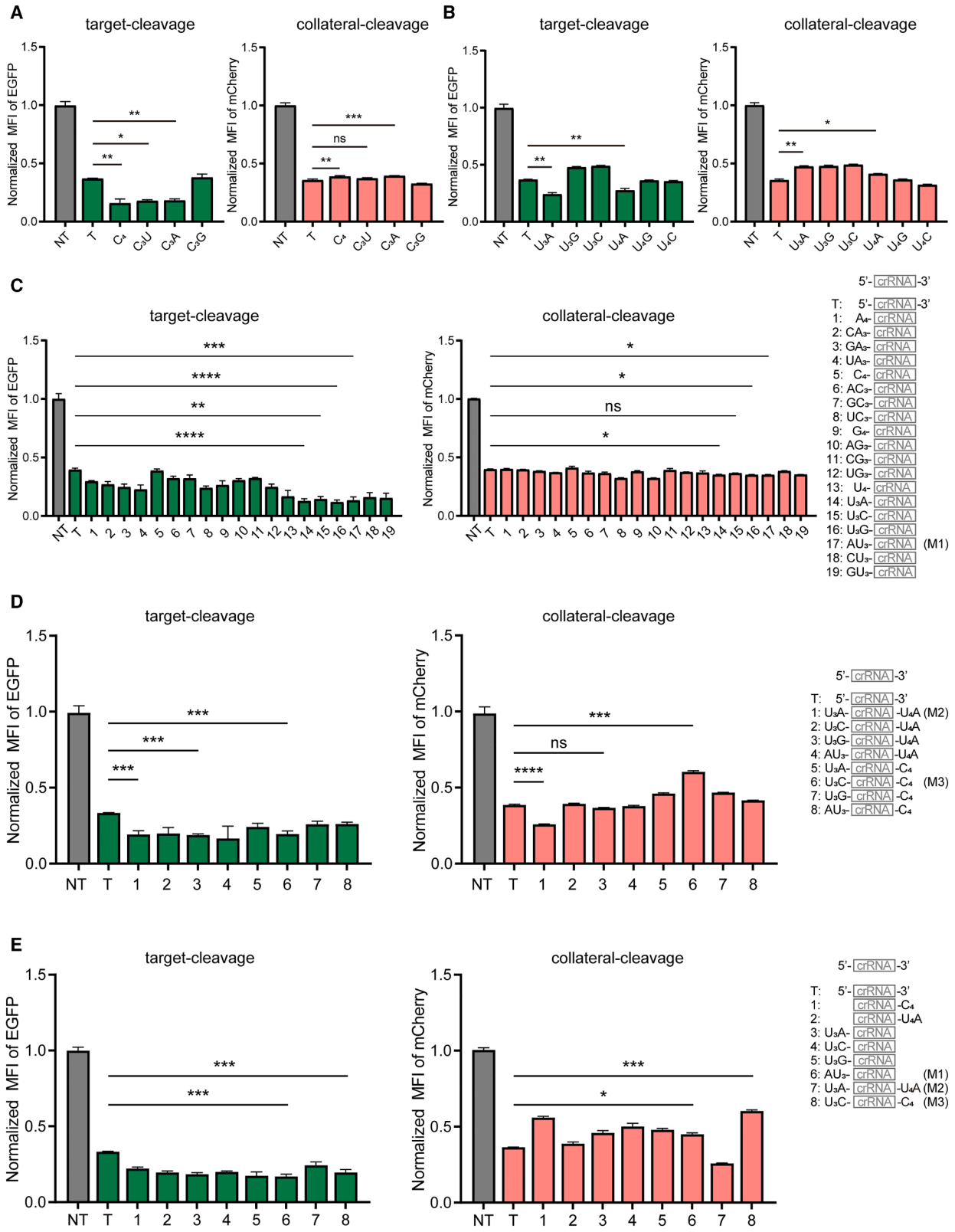
Given previous reports of CRISPR-Cas-system-mediated antiviral effects,[12,14,26] we investigated the inhibitory efficiency of our designed CRISPR-Cas13a system on the replication of mumps virus (MuV), a common respiratory virus that causes epidemic parotitis and damages the human reproductive and nervous systems.[40,41] Conserved target sites in the HN and P genes were selected via multiple sequences alignment and RNA structure prediction. Finally, two crRNAs were designed for each gene based on those sites. Vero-E6 cells infected with MuV were introduced with our designed CRISPR-Cas13a system, and the viral load in the supernatants was measured by qPCR. When targeting HN, the inhibitory efficiency of enCas13a with wt crRNA, M1crRNA, or M3crRNA was increased by at least 20%, 10%, and 3%, respectively, compared to the WT group (Figure 6C). Similarly, P gene-targeting crRNAs significantly reduced viral titers in the supernatant of infected cultures (Figure 6D), confirming the antiviral capacity of our designed CRISPR-Cas13a system.

Mechanism exploration of engineered CRISPR-Cas13a systems

To examine the molecular foundation of the enhanced knockdown efficacy of our engineered CRISPR-Cas13a system, we purified Cas13a(wt), enCas13a, wt crRNA, M1crRNA, and M3crRNA, followed by biolayer interferometry (BLI) to assess binding kinetics. BLI analysis revealed that both enCas13a and the modified crRNAs independently increased binding affinity within the RNP complex (Figures 7A and 7B). Interestingly, the enhancement in binding affinity was less pronounced when enCas13a was combined with modified crRNAs than when wild-type Cas13a was paired with the same crRNAs. The plateau effect may indicate a saturation point in binding enhancement, implying that the modified Cas13a and crRNA components collectively reach the maximum turnover efficiency. Overall, these results indicate that enCas13a strengthens crRNA binding, with the highest affinity observed in combination with M3crRNA.

Figure 3. Schematic diagram of crRNA optimization

(A) Secondary structure and terminal extension strategies of crRNA. Red characters represent repeat regions, blue characters spacer regions, and purple characters terminal extensions. (B) Exploration of the optimal crRNA spacer length. Data were analyzed using the Kruskal-Wallis test followed by Dunn's multiple comparisons test, comparing each group to the non-targeting (NT) crRNA control. Data are presented as median ± IQR ($n = 4$). ***$p < 0.001$; ****$p < 0.0001$; ns, not significant.



(legend on next page)

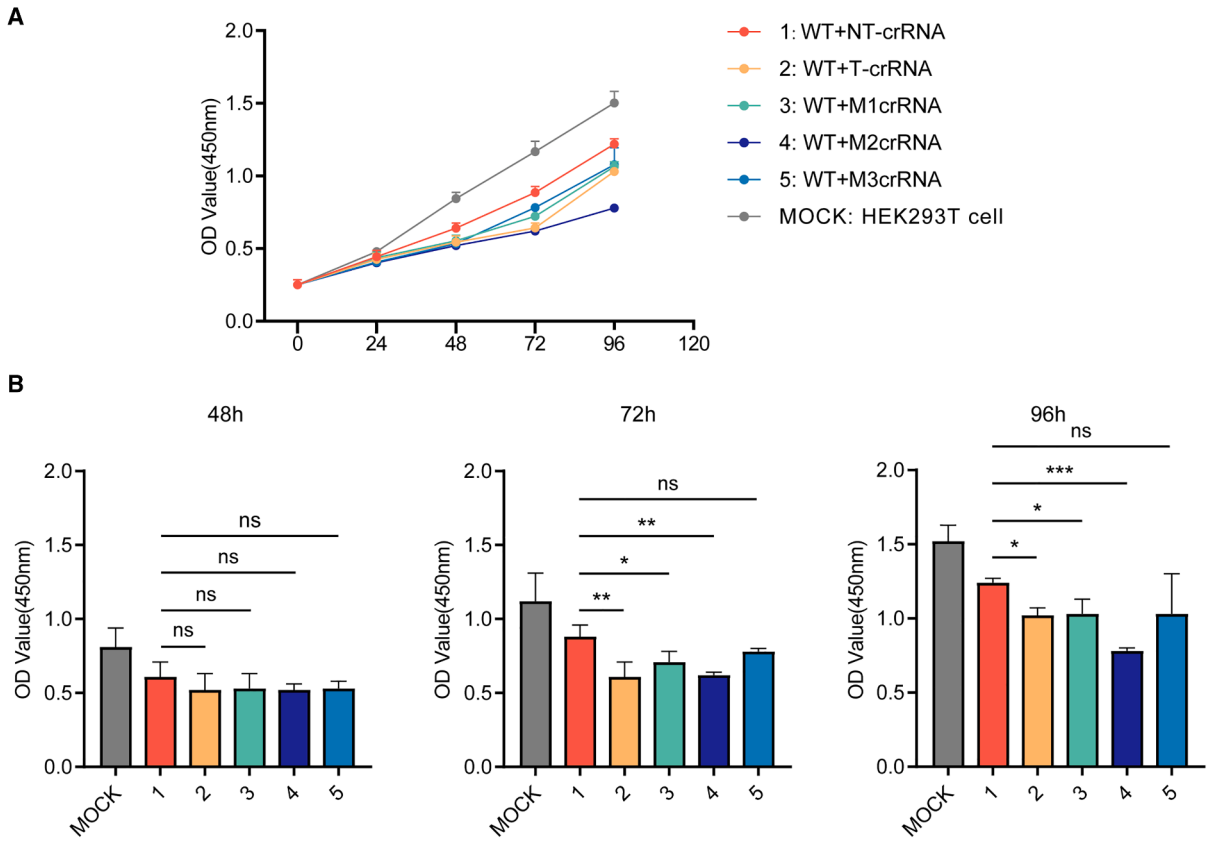


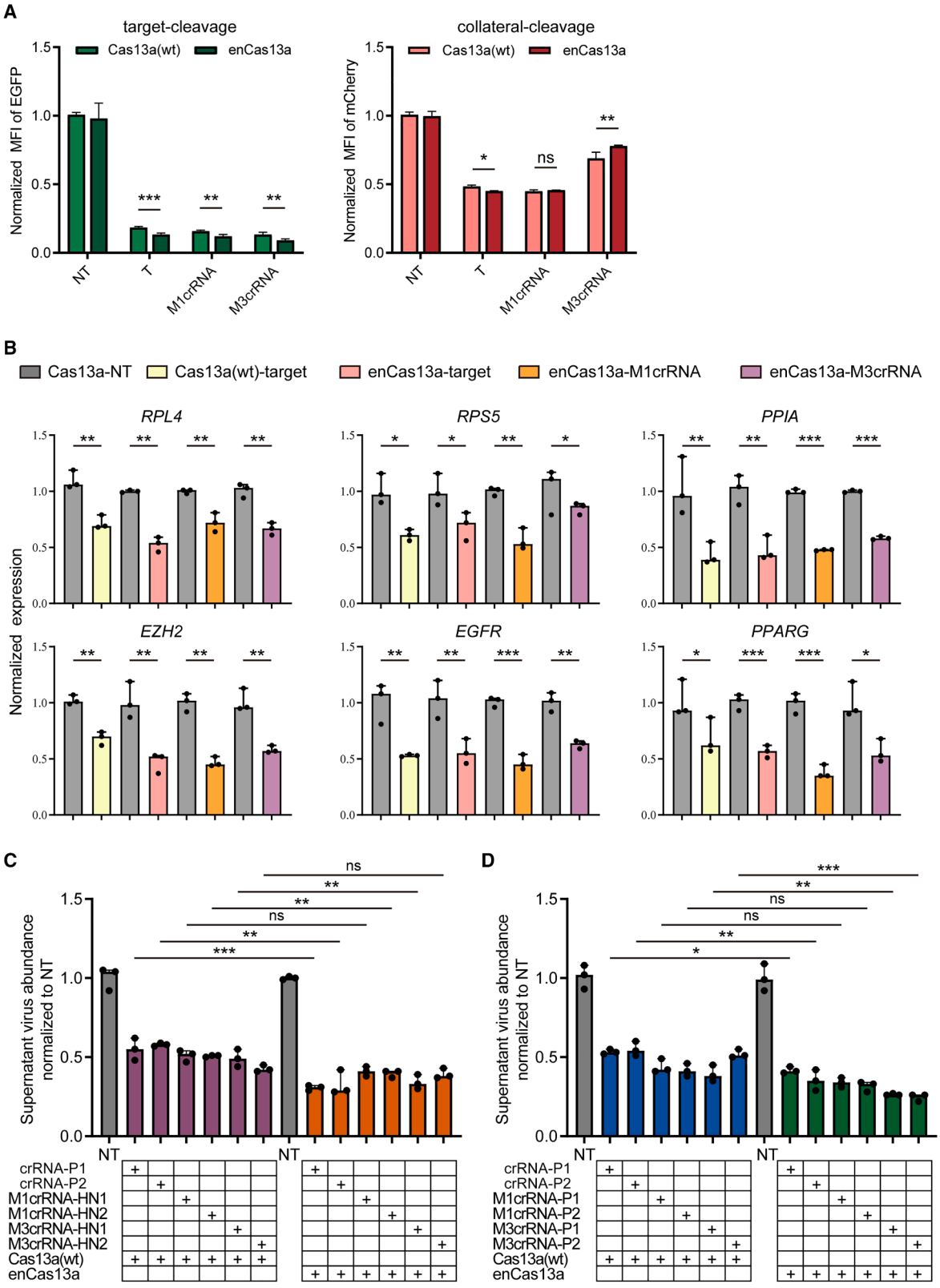
Figure 5. Cytotoxicity evaluation of CRISPR-Cas13a system with engineered crRNAs

(A) Cell viability was determined using CCK-8 reagent at 24, 48, 72, and 96 h post-transfection. The line chart is the overall graph. WT, wild-type LwaCas13a; NT-crRNA, nontarget crRNA; T-crRNA, target crRNA. (B) Bar charts show specific data for each time point. Data were compared using a two-tailed unpaired Mann-Whitney U test. Data are presented as median ± IQR (n = 3). *p < 0.05; **p < 0.01; ***p < 0.001; ns, not significant.

To further assess if the improved knockdown efficacy is structurally influenced by modified protein-RNA interactions, we performed structural modeling using AlphaFold to predict the structure of Cas13a(wt)-wt crRNA, enCas13a-wt crRNA, and enCas13a-M3crRNA binary complexes. Molecular visualizations were generated with PyMOL, and nucleotide positions in wt crRNA and M3crRNA were annotated (Figure S3). Focusing on residues Q521, E796, and E810, the mutated sites in enCas13a, we analyzed local protein-RNA interactions within the predicted complex structures. In the Cas13a(wt)-wt crRNA complex, nucleotides A(35), A(38), C(39), and G(41) interacted with residues Tyr597, Asn660, Asn802, and Arg1133, respectively. In contrast, the enCas13a-wt crRNA complex exhibited expanded contact points: nucleotides A(34), C(36), C(37), A(38), U(40), G(41), and C(42) interact with residues Ser557, Phe558, Lys560, Lys582, Lys593, Tyr597, Asn660, Lys666, Lys770, Arg807, Arg855, and Arg961 (Figure 8A). This extended interaction network suggests that mutations Q521R, E796A, and E810A lead to a more compact and conformationally stabilized binary complex. While the enCas13a-M3crRNA complex showed minimal global conformational change compared to Cas13a(wt)-wt crRNA complex, the M3crRNA itself experienced a significant structural transition toward the protein core, increasing its contact area with the Cas13a surface (Figure 8B). These observations suggest that enCas13a remodels the protein-RNA interface to promote tighter binding, while M3crRNA's altered secondary structure further facilitates complex formation by broadening the interaction network.

Figure 4. Screening and performance of crRNA mutants

(A) The targeted (EGFP) and collateral (mCherry) cleavage activities of Cas13a combined with crRNA mutants with 3' end C_3N extensions. (B) The targeted (EGFP) and collateral (mCherry) cleavage activities of Cas13a combined with crRNA mutants with 3' end U_3V (A/C/G) or U_4V (A/C/G) extensions. (C) The targeted (EGFP) and collateral (mCherry) cleavage activities of Cas13a combined with crRNA mutants with 5' end N_4 extensions. (D) The targeted (EGFP) and collateral (mCherry) cleavage activities of Cas13a combined with crRNA mutants with both 5' and 3' end beneficial extensions. (E) The targeted (EGFP) and collateral (mCherry) cleavage activities of Cas13a combined with all the beneficial crRNA mutants. Data were analyzed using the Kruskal-Wallis test followed by Dunn's multiple comparisons test, comparing each group to the non-targeting (NT) crRNA control. Data are presented as median ± IQR (n = 4). *p < 0.05; **p < 0.01; ***p < 0.001; ****p < 0.0001; ns, not significant.



(legend on next page)

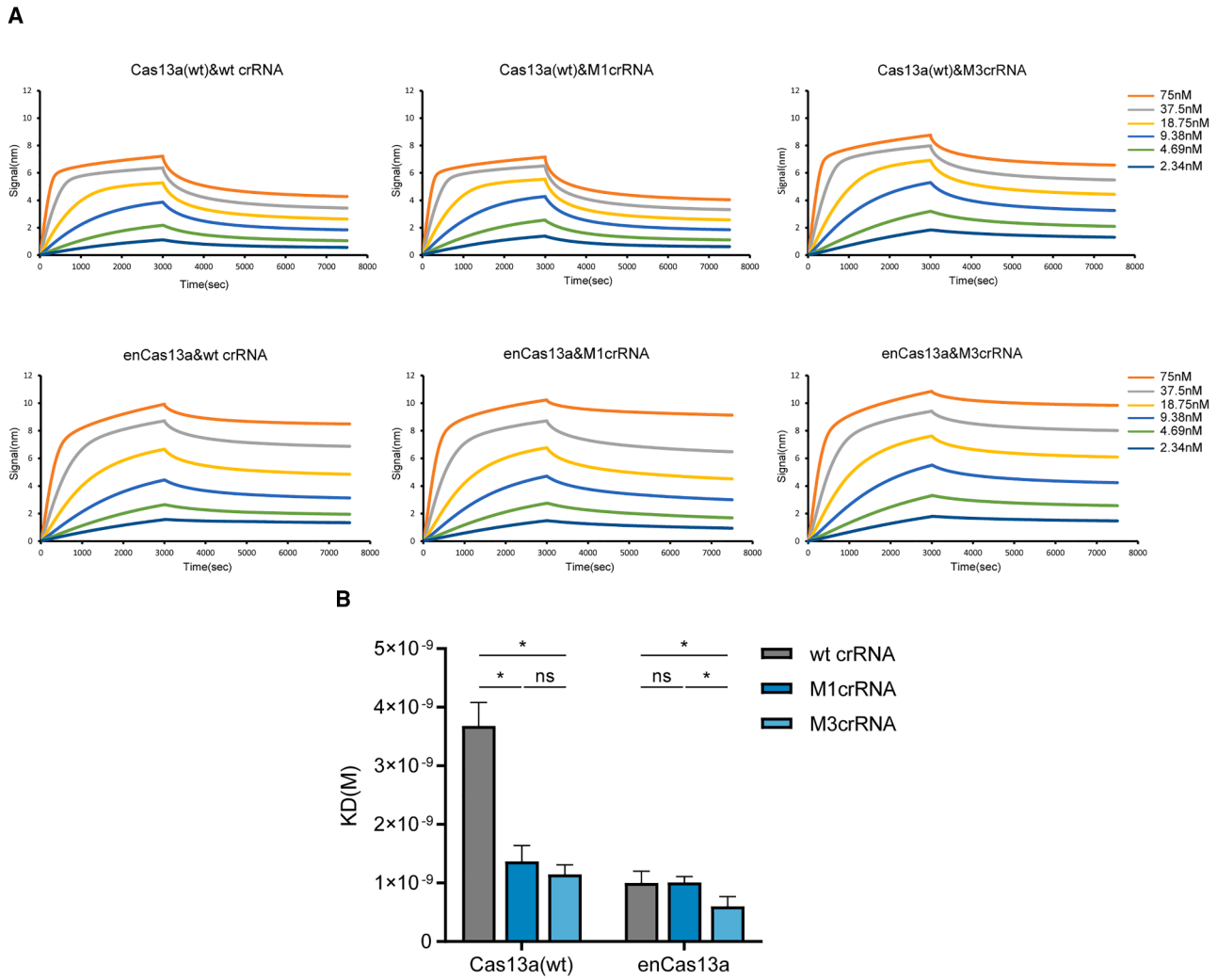


Figure 7. Engineered Cas13a mutant and crRNA mutants contribute to enhancing Cas-crRNA interactions

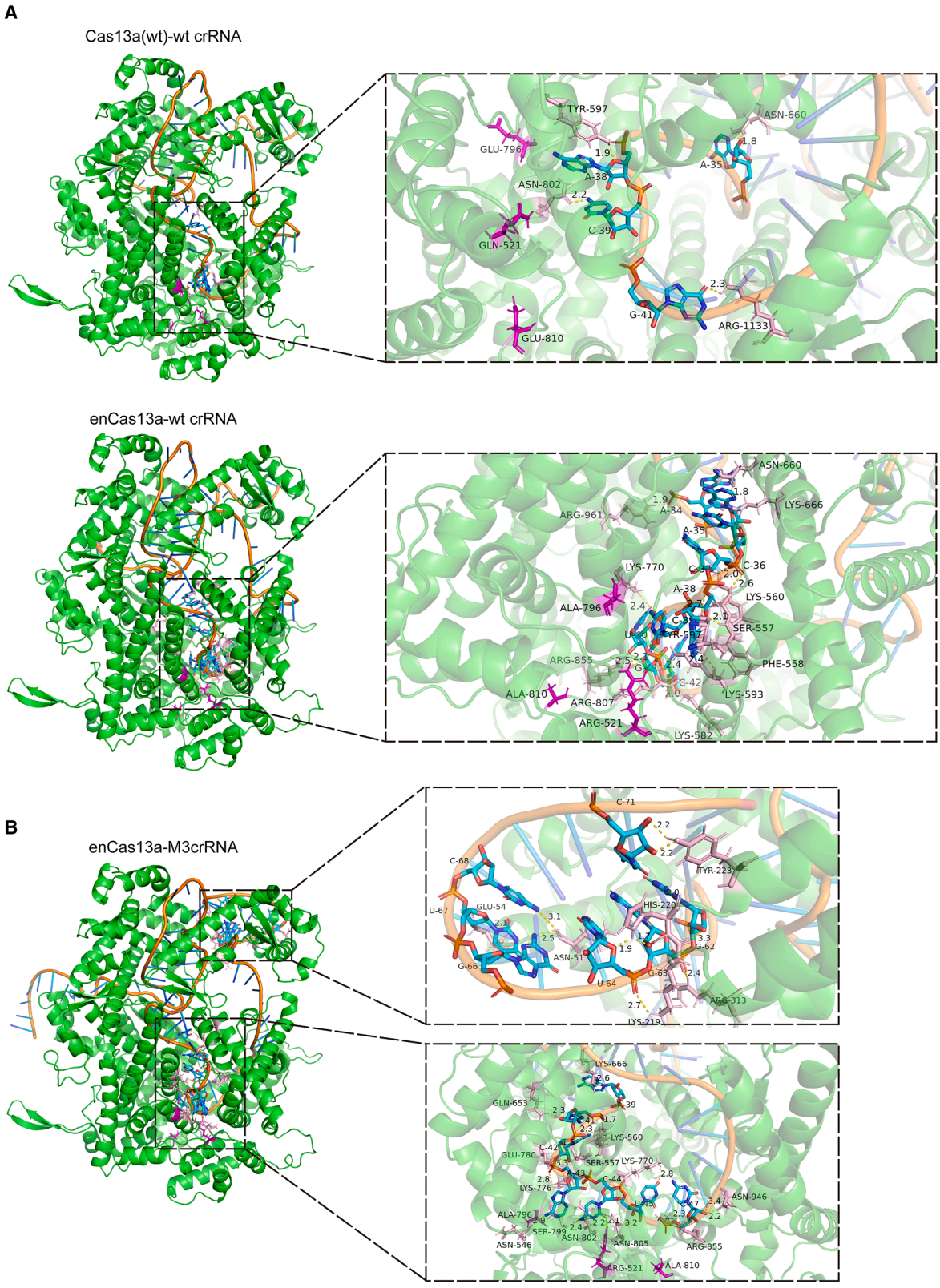
(A) BLI kinetic analysis of the interaction between wild-type/mutant Cas13a and wild-type/mutant crRNAs. Kinetic parameters were from a 1:1 binding model. (B) Comparison of the KD values in graph A. Data were compared using a two-tailed unpaired Mann-Whitney U test. Data are presented as median ± IQR ($n = 4$). *$p < 0.05$; ns, not significant.

DISCUSSION

The CRISPR-Cas system has become an essential tool in gene editing, diagnostics, and synthetic biology. Cas13a, as the first RNA-targeting CRISPR effector, offers unique advantages over DNA-editing systems like Cas9, particularly in safety and reversibility. Recent studies have demonstrated that collateral activity is highly dependent on the environment, being more pronounced in scenarios with high RNA abundance (e.g., tumor cells) or in the presence of overexpressed exogenous genes. While this activity can inhibit tumor cell growth and induce apoptosis, in mammalian cells undergoing RNA knockdown or antiviral experiments, no collateral activities were detected between target and non-target cells, with no impact on cellular viability.[8,14,18,42] These findings suggest that the intracellular environment and RNA localization can influence the threshold and consequences of collateral activity. Therefore, compared to the wild-type Cas13a system, an engineered Cas13a system with enhanced on-target activity and reduced collateral activity should carry a lower risk *in vivo*, significantly improving its potential for therapeutic applications.

Figure 6. Engineered CRISPR-Cas13a system exhibits superior cleavage activity in mammalian cells

(A) Cleavage activity was determined by dual fluorescence system in HEK293T cells. NT, nontarget crRNA; T, target crRNA ($n = 4$). (B) Knockdown efficiency of six endogenous transcripts was determined by qPCR ($n = 3$). (C and D) Antiviral assays targeting MuV HN (left) and P (right) genes. Viral titers in Vero-E6 cell supernatants were determined by qPCR ($n = 3$). Data were compared using a two-tailed unpaired Mann-Whitney U test. Data are presented as median ± IQR. *$p < 0.05$; **$p < 0.01$; ***$p < 0.001$; ns, not significant.



(legend on next page)

In this study, we employed structure-guided design and site-directed mutagenesis to generate a triple mutant of LwaCas13a (Q521R/E796A/E810A), termed enCas13a. Compared to wild-type Cas13a, enCas13a exhibited a 14.67% increase in targeted cleavage efficiency, accompanied by a relatively modest 8% rise in collateral cleavage activity. Previous studies have shown that TA-rich extensions can improve the performance of CRISPR-Cas system.[33–35,43] Based on this concept, we designed crRNA variants incorporating 5' and 3' end modifications. These modifications improved targeted cleavage activity, with little effect on collateral cleavage activity (in the case of M1crRNA) and even reduced collateral cleavage activity (in the case of M3crRNA). This is the first time that dual-end modification of crRNA has been achieved within the Cas13a system. When combined with enCas13a, M1crRNA and M3crRNA significantly enhanced knockdown efficiency across both exogenous and endogenous genes. Notably, this synergy was most pronounced for low-abundance genes, such as PPARG and EZH2, highlighting the value of engineered systems in difficult-to-target transcripts. Moreover, the engineered CRISPR-Cas13a system retained its antiviral capabilities and effectively suppressed MuV replication in mammalian cells. Our system achieved up to 20% improvement in viral RNA knockdown, further supporting its potential for therapeutic antiviral applications.

Mechanistic analyses suggested that the enhanced cleavage efficiency is attributable to two major factors: (1) increased crRNA-Cas13a binding affinity, as demonstrated by BLI assays, and (2) altered binary complex architecture, as predicted by AlphaFold modeling. The BLI results conclusively show that the modified crRNA variants exhibiting enhanced knockdown efficiency in our cellular assays indeed possess a stronger binding affinity (a lower KD value) for enCas13a compared to the wild-type crRNA. Compared to the wild-type complex, the enCas13a-crRNA binary complex displayed a more compact conformation with a wider range of protein-RNA contacts, especially around the mutation sites (Q521, E796, and E810). Similarly, the M3crRNA conformation shifted toward the protein core, increasing structural engagement. This finding is consistent with previous studies showing that alteration of the crRNA influences cleavage activity and RNP stability.[7,39] Importantly, M3crRNA not only improved targeted activity but also reduced collateral activity, a phenomenon that remains incompletely understood. One possibility is that its altered secondary structure occludes access to the HEPN1/2 domains (the RNase active cavity), preventing the entry of non-target RNA. Taken together, this strong correlation between the AlphaFold-predicted conformational changes, the observed increase in binding affinity (BLI), and the improved target knockdown efficiency provides robust, multifaceted validation of our model and confirms the reliability of the engineered Cas13a system.

This study also presents certain issues and limitations. The performance of the enCas13a system has only been validated under *in vitro* conditions. Future research of testing its efficacy in more complex physiological environments, such as animal models, is needed to comprehensively assess its specificity, durability, and safety. Mechanistically, our analyses provide preliminary evidence for strengthened Cas protein-crRNA interactions. Subsequently, high-resolution structural studies (cryo-EM) together with kinetic assays and transcriptome-wide assays will be employed to elucidate the fundamental mechanisms underlying this increased activity.

In summary, we report a synergistic strategy that combines Cas13a protein engineering with rational crRNA design to achieve improved RNA targeting and reduced collateral effects. The optimization ideas and modification methods used in this study can also provide insights and direction for other researchers in this field when developing new CRISPR-Cas tools. The enCas13a-M3crRNA combination provides a robust, customizable, and safer RNA-targeting system for diverse applications ranging from transcript knockdown to antiviral defense. Future investigations should focus on elucidating the structural basis for collateral activity suppression and adapting this platform to other Cas13 orthologs.

MATERIALS AND METHODS

Plasmid construction

Human codon-optimized Cas13a expression plasmid was obtained from Addgene (#90097). Cas13a variants and crRNA sequences were cloned using homologous recombination with ClonExpress II One Step Cloning Kit (Vazyme) or 2× Ezmax Universal CloneMix (TOLOBIO). PCR amplifications were performed using 2× Phanta Flash Master Mix (Vazyme) according to manufacturer's instructions. All constructs were verified by Sanger sequencing. Detailed sequences are provided in Tables S1 and S2.

Cell culture, transfection, and flow cytometry analysis

HEK293T and Vero-E6 cell lines were cultured in DMEM (Gibco) supplemented with 10% FBS (Sijiqing) at 37°C in 5% CO_2. For cleavage assays, cells were seeded in 48-well plates and transfected with Cas13a and crRNA plasmids at a 3:2 molar ratio using polyethyleneimine (PEI), while a 1:3 ratio of DNA to PEI was maintained. EGFP and mCherry fluorescence were quantified 48 h post-transfection using a Beckman CytoFLEX S flow cytometer. Data were then processed and interpreted with FlowJo software (v.10.8.1).

Viral propagation, titration, and infection

Vero-E6 cells were seeded in 60-mm cell culture dish 1–2 days prior to infection and maintained in DMEM with 10% FBS. Viral stocks were thawed on ice, and 200 μL was used to inoculate each well. Inoculation was performed for 1 h with rocking every 20 min.

Figure 8. Structural modeling of wild-type and engineered CRISPR-Cas13a system

(A) Structural diagram of the binary complex between wild-type/mutant Cas13a and wild-type crRNA, along with a local magnification. (B) Structural diagram of the binary complex between mutant Cas13a and M3crRNA, along with a local magnification. Mutant amino acid residues are labeled in rose; amino acid residues in contact with the 34th to 42nd bases of crRNA are labeled in pink.

Supernatants were collected after 48 h, filtered through a 0.22 μm membrane, aliquoted, and stored at −80°C.

Mumps virus (MuV) titer was determined via $TCID_{50}$ assay using Vero-E6 cells. Cells were seeded in 96-well plates to form a monolayer. Virus stocks were diluted in a 10-fold gradient in DMEM, and 100 μL of each dilution was added per well. After 1 h of adsorption, cytopathic effects (CPEs) were monitored over 72 h. Titers were calculated by the Reed-Muench method.

For antiviral experiments, Vero-E6 cells were seeded in 96-well plates and transfected using Hieff Trans Liposomal Transfection Reagent (Yeasen, China) at a 3:2 ratio of Cas13a to crRNA plasmids. A 1:3 ratio of DNA to transfection reagent was maintained. After 24 h, cells were infected with MuV at MOI = 0.1 for 1 h, followed by incubation in DMEM containing 2% FBS at 37°C for 72 h. Supernatants were then collected for viral load quantification.

Total RNA harvest and quantitative PCR

Cells were harvested 48 h after transfection for endogenous gene analysis. Total RNA was extracted with total RNA extraction reagent (Vazyme). For viral RNA detection, supernatants were collected 72 h after viral infection, and total RNA was subsequently extracted using a GeneRotex 96 Nucleic Acid Extractor. Reverse transcription was performed using PrimeScript RT Master Mix (Takara). qPCR was conducted using 2× HQ SYBR qPCR Mix (ZOMANBIO). Endogenous gene expression was analyzed via the $2^{-\Delta\Delta Ct}$ method, which determines the relative expression level of the target gene by calculating the average CT value difference between the target gene and the reference gene GAPDH across three biological replicates. Each experimental group was normalized against its corresponding control group, while viral RNA levels were quantified using absolute quantification. Primer sequences are listed in Table S3.

Cas13a protein expression and purification

The expression plasmid for Cas13a was transformed into Rosetta 2(DE3) pLysS competent cells (WEIDI). A 40 mL starter culture grew overnight in Luria-Bertani growth media (LB), which was used to inoculate 4 L of LB. Cells were grown at 37°C until OD_{600} reached 0.6, then induced with 500 μM IPTG and incubated at 18°C for 16 h. Cells were pelleted by centrifugation (8,000 × g, 15 min, 4°C) and stored at −80°C prior to purification.

All purification steps were consistent with previous studies.[22] Briefly, lysis buffer (20 mM Tris-HCl, 500 mM NaCl, 1 mM DTT, pH 8.0) was used to resuspend the cell pellet, and the resuspension was subsequently lysed by a low-temperature ultra-high-pressure cell crusher (JNBIO). The lysate was centrifuged (25,000 × g, 1 h, 4°C), and the supernatant was incubated with 3 mL of Strep-Tactin XT Sepharose (GE Healthcare) and rotated at 4°C for 40 min. After elution and ULP1 cleavage, the protein was subjected to buffer exchange through a HiPrep 26/10 Desalting column (GE Healthcare) and eluted by Buffer A (20 mM Tris-HCl, 1 mM DTT, 5% glycerol, pH 8.0). Proteins were further purified on a Resource S column (GE Healthcare) with NaCl gradient (130 mM–2 M), then subjected to SDS-PAGE. Fractions containing Cas13a were pooled and exchanged into storage buffer (600 mM NaCl, 50 mM TrisHCl pH 7.5, 5% glycerol, 2 mM DTT) and stored at −80°C.

In vitro transcription and purification of crRNA

The DNA templates used for crRNA transcription were obtained by PCR using KOD-Plus-Neo (TOYOBO) and purified by a phenol-chloroform extraction method followed by ethanol precipitation. Biotin-modified crRNAs were prepared by *in vitro* transcription using the Biotin RNA Labeling Kit (Beyotime). The procedure was carried out according to the manufacturer's instructions. The crRNAs were then purified by phenol-chloroform extraction and ethanol precipitation and dissolved in nuclease-free water. Biotin-modified crRNAs are listed in Table S2.

Biolayer interferometry binding kinetic assay

The BLI experimental procedure is consistent with our previous work.[44] In brief, the binding affinity between the Cas13a protein and crRNAs was quantitatively assessed using the Octet RED96 instrument (ForteBio) at 30°C with a shaking speed of 1,000 RPM. Streptavidin biosensors were hydrated in BLI buffer (10 mM HEPES, pH = 7.0, 150 mM NaCl, 1%BSA [w/v], 0.02%Tween 20 [v/v]) for a minimum of 15 min, followed by a 120-s equilibration with BLI buffer. Subsequently, 100 nM crRNAs were diluted in BLI buffer and loaded onto the biosensor surfaces for 400 s. After 120 s of baseline equilibration, 600 s of association was performed using Cas13a proteins at concentrations ranging from 2 to 300 nM, followed by 900 s of dissociation in the same buffer. Data were normalized by subtracting the signals obtained from reference samples. A 1:1 binding model with a global fit approach was used to calculate the equilibrium dissociation constants (KD). GraphPad Prism 9 software was used for statistical analysis.

Cell viability assay

Cell viability was determined using Cell Counting Kit-8 (CCK-8) (Beyotime) according to the manufacturer's protocol. Briefly, cells were seeded overnight in 96-well plates at a density of 1,000 cells per well. The plasmids of Cas13a protein and crRNA were co-transfected into the cells using PEI. At 24, 48, 72, and 96 h post-transfection, 10% CCK-8 solution (v/v) was added and incubated for 1.5 h at 37°C. Absorbance at 450 nm was measured using a microplate reader.

Structural prediction

The full-length amino sequences of wild-type LwaCas13a and its variant enCas13a were submitted to the AlphaFold server for structure predictions using default parameters.

Statistical analysis

All experiments were repeated at least three times unless otherwise specified. Statistical analyses were conducted using GraphPad Prism 9. Two-tailed unpaired Mann-Whitney U test was used for two-group comparisons, and Kruskal-Wallis test followed by Dunn's

multiple comparisons test was used for multi-group analyses. Data are presented as median ± IQR for non-parametric methods. Phylogenetic tree analysis of Cas13a was performed in MEGA11 using neighbor-joining method of inference.[45,46] Statistical significance was defined as $^{*}p < 0.05$, $^{**}p < 0.01$, $^{***}p < 0.001$, and $^{****}p < 0.0001$.

DATA AND CODE AVAILABILITY

The data supporting the findings of this study are provided within the article and its supplemental information. Further detailed information is available from the corresponding author on reasonable request.

ACKNOWLEDGMENTS

This research received no financial support from any commercial organization or funding agency with a potential conflict of interest for the work described in this paper.

AUTHOR CONTRIBUTIONS

W.Z., data curation, formal analysis, investigation, methodology, and writing—original draft. H.W., investigation and methodology. D.L., software and visualization. X.M., data curation and software. Y.Z., investigation and validation. Y.Y., investigation and validation. Z.L., methodology. T.P., validation. Y.L., conceptualization, resources, supervision, and writing—review & editing. Q.Z., project administration, supervision, and writing—review & editing.

DECLARATION OF INTERESTS

The authors declare no competing interests.

SUPPLEMENTAL INFORMATION

Supplemental information can be found online at https://doi.org/10.1016/j.omtn.2025.102811.

REFERENCES

1. Horvath, P., and Barrangou, R. (2010). CRISPR/Cas, the immune system of bacteria and archaea. Science *327*, 167–170.
2. Shmakov, S., Abudayyeh, O.O., Makarova, K.S., Wolf, Y.I., Gootenberg, J.S., Semenova, E., Minakhin, L., Joung, J., Konermann, S., Severinov, K., et al. (2015). Discovery and Functional Characterization of Diverse Class 2 CRISPR-Cas Systems. Mol. Cell *60*, 385–397.
3. Makarova, K.S., Wolf, Y.I., Iranzo, J., Shmakov, S.A., Alkhnbashi, O.S., Brouns, S.J.J., Charpentier, E., Cheng, D., Haft, D.H., Horvath, P., et al. (2020). Evolutionary classification of CRISPR-Cas systems: a burst of class 2 and derived variants. Nat. Rev. Microbiol. *18*, 67–83.
4. Yang, H., and Patel, D.J. (2024). Structures, mechanisms and applications of RNA-centric CRISPR-Cas13. Nat. Chem. Biol. *20*, 673–688.
5. Abudayyeh, O.O., Gootenberg, J.S., Konermann, S., Joung, J., Slaymaker, I.M., Cox, D.B.T., Shmakov, S., Makarova, K.S., Semenova, E., Minakhin, L., et al. (2016). C2c2 is a single-component programmable RNA-guided RNA-targeting CRISPR effector. Science *353*, aaf5573.
6. Li, S.-Y., Cheng, Q.-X., Liu, J.-K., Nie, X.-Q., Zhao, G.-P., and Wang, J. (2018). CRISPR-Cas12a has both cis- and trans-cleavage activities on single-stranded DNA. Cell Res. *28*, 491–493.
7. Liu, L., Li, X., Ma, J., Li, Z., You, L., Wang, J., Wang, M., Zhang, X., and Wang, Y. (2017). The Molecular Architecture for RNA-Guided RNA Cleavage by Cas13a. Cell *170*, 714–726.e10.
8. Abudayyeh, O.O., Gootenberg, J.S., Essletzbichler, P., Han, S., Joung, J., Belanto, J.J., Verdine, V., Cox, D.B.T., Kellner, M.J., Regev, A., et al. (2017). RNA targeting with CRISPR-Cas13. Nature *550*, 280–284.
9. Konermann, S., Lotfy, P., Brideau, N.J., Oki, J., Shokhirev, M.N., and Hsu, P.D. (2018). Transcriptome Engineering with RNA-Targeting Type VI-D CRISPR Effectors. Cell *173*, 665–676.e14.
10. Aman, R., Ali, Z., Butt, H., Mahas, A., Aljedaani, F., Khan, M.Z., Ding, S., and Mahfouz, M. (2018). RNA virus interference via CRISPR/Cas13a system in plants. Genome Biol. *19*, 1.
11. Kushawah, G., Hernandez-Huertas, L., Abugattas-Nuñez Del Prado, J., Martinez-Morales, J.R., DeVore, M.L., Hassan, H., Moreno-Sanchez, I., Tomas-Gallardo, L., Diaz-Moscoso, A., Monges, D.E., et al. (2020). CRISPR-Cas13d Induces Efficient mRNA Knockdown in Animal Embryos. Dev. Cell *54*, 805–817.e7.
12. Abbott, T.R., Dhamdhere, G., Liu, Y., Lin, X., Goudy, L., Zeng, L., Chemparathy, A., Chmura, S., Heaton, N.S., Debs, R., et al. (2020). Development of CRISPR as an Antiviral Strategy to Combat SARS-CoV-2 and Influenza. Cell *181*, 865–876.e12.
13. Blanchard, E.L., Vanover, D., Bawage, S.S., Tiwari, P.M., Rotolo, L., Beyersdorf, J., Peck, H.E., Bruno, N.C., Hincapie, R., Michel, F., et al. (2021). Treatment of influenza and SARS-CoV-2 infections via mRNA-encoded Cas13a in rodents. Nat. Biotechnol. *39*, 717–726.
14. Freije, C.A., Myhrvold, C., Boehm, C.K., Lin, A.E., Welch, N.L., Carter, A., Metsky, H.C., Luo, C.Y., Abudayyeh, O.O., Gootenberg, J.S., et al. (2019). Programmable Inhibition and Detection of RNA Viruses Using Cas13. Mol. Cell *76*, 826–837.e11.
15. Xu, C., Zhou, Y., Xiao, Q., He, B., Geng, G., Wang, Z., Cao, B., Dong, X., Bai, W., Wang, Y., et al. (2021). Programmable RNA editing with compact CRISPR-Cas13 systems from uncultivated microbes. Nat. Methods *18*, 499–506.
16. East-Seletsky, A., O'Connell, M.R., Burstein, D., Knott, G.J., and Doudna, J.A. (2017). RNA Targeting by Functionally Orthogonal Type VI-A CRISPR-Cas Enzymes. Mol. Cell *66*, 373–383.e3.
17. Buchman, A.B., Brogan, D.J., Sun, R., Yang, T., Hsu, P.D., and Akbari, O.S. (2020). Programmable RNA Targeting Using CasRx in Flies. CRISPR J. *3*, 164–176.
18. Wang, Q., Liu, X., Zhou, J., Yang, C., Wang, G., Tan, Y., Wu, Y., Zhang, S., Yi, K., and Kang, C. (2019). The CRISPR-Cas13a Gene-Editing System Induces Collateral Cleavage of RNA in Glioma Cells. Adv. Sci. *6*, 1901299.
19. Ai, Y., Liang, D., and Wilusz, J.E. (2022). CRISPR/Cas13 effectors have differing extents of off-target effects that limit their utility in eukaryotic cells. Nucleic Acids Res. *50*, e65.
20. Li, Y., Xu, J., Guo, X., Li, Z., Cao, L., Liu, S., Guo, Y., Wang, G., Luo, Y., Zhang, Z., et al. (2023). The collateral activity of RfxCas13d can induce lethality in a RfxCas13d knock-in mouse model. Genome Biol. *24*, 20.
21. Cox, D.B.T., Gootenberg, J.S., Abudayyeh, O.O., Franklin, B., Kellner, M.J., Joung, J., and Zhang, F. (2017). RNA editing with CRISPR-Cas13. Science *358*, 1019–1027.
22. Gootenberg, J.S., Abudayyeh, O.O., Lee, J.W., Essletzbichler, P., Dy, A.J., Joung, J., Verdine, V., Donghia, N., Daringer, N.M., Freije, C.A., et al. (2017). Nucleic acid detection with CRISPR-Cas13a/C2c2. Science *356*, 438–442.
23. Gootenberg, J.S., Abudayyeh, O.O., Kellner, M.J., Joung, J., Collins, J.J., and Zhang, F. (2018). Multiplexed and portable nucleic acid detection platform with Cas13, Cas12a, and Csm6. Science *360*, 439–444.
24. Myhrvold, C., Freije, C.A., Gootenberg, J.S., Abudayyeh, O.O., Metsky, H.C., Durbin, A.F., Kellner, M.J., Tan, A.L., Paul, L.M., Parham, L.A., et al. (2018). Field-deployable viral diagnostics using CRISPR-Cas13. Science *360*, 444–448.
25. Zhou, T., Huang, R., Huang, M., Shen, J., Shan, Y., and Xing, D. (2020). CRISPR/Cas13a Powered Portable Electrochemiluminescence Chip for Ultrasensitive and Specific MiRNA Detection. Adv. Sci. *7*, 1903661.
26. Li, H., Wang, S., Dong, X., Li, Q., Li, M., Li, J., Guo, Y., Jin, X., Zhou, Y., Song, H., and Kou, Z. (2020). CRISPR-Cas13a Cleavage of Dengue Virus NS3 Gene Efficiently Inhibits Viral Replication. Mol. Ther. Nucleic Acids *19*, 1460–1469.
27. East-Seletsky, A., O'Connell, M.R., Knight, S.C., Burstein, D., Cate, J.H.D., Tjian, R., and Doudna, J.A. (2016). Two distinct RNase activities of CRISPR-C2c2 enable guide-RNA processing and RNA detection. Nature *538*, 270–273.
28. Kiga, K., Tan, X.-E., Ibarra-Chávez, R., Watanabe, S., Aiba, Y., Sato'o, Y., Li, F.-Y., Sasahara, T., Cui, B., Kawauchi, M., et al. (2020). Development of CRISPR-Cas13a-based antimicrobials capable of sequence-specific killing of target bacteria. Nat. Commun. *11*, 2934.
29. Kleinstiver, B.P., Sousa, A.A., Walton, R.T., Tak, Y.E., Hsu, J.Y., Clement, K., Welch, M.M., Horng, J.E., Malagon-Lopez, J., Scarfò, I., et al. (2019). Engineered CRISPR-Cas12a variants with increased activities and improved targeting ranges for gene, epigenetic and base editing. Nat. Biotechnol. *37*, 276–282.

30. Ma, E., Chen, K., Shi, H., Stahl, E.C., Adler, B., Trinidad, M., Liu, J., Zhou, K., Ye, J., and Doudna, J.A. (2022). Improved genome editing by an engineered CRISPR-Cas12a. Nucleic Acids Res. *50*, 12689–12701.

31. Kato, K., Zhou, W., Okazaki, S., Isayama, Y., Nishizawa, T., Gootenberg, J.S., Abudayyeh, O.O., and Nishimasu, H. (2022). Structure and engineering of the type III-E CRISPR-Cas7-11 effector complex. Cell *185*, 2324–2337.e16.

32. Yang, J., Song, Y., Deng, X., Vanegas, J.A., You, Z., Zhang, Y., Weng, Z., Avery, L., Dieckhaus, K.D., Peddi, A., et al. (2023). Engineered LwaCas13a with enhanced collateral activity for nucleic acid detection. Nat. Chem. Biol. *19*, 45–54.

33. Park, H.M., Liu, H., Wu, J., Chong, A., Mackley, V., Fellmann, C., Rao, A., Jiang, F., Chu, H., Murthy, N., and Lee, K. (2018). Extension of the crRNA enhances Cpf1 gene editing in vitro and in vivo. Nat. Commun. *9*, 3313.

34. Nguyen, L.T., Smith, B.M., and Jain, P.K. (2020). Enhancement of trans-cleavage activity of Cas12a with engineered crRNA enables amplified nucleic acid detection. Nat. Commun. *11*, 4906.

35. Yang, Y., Sun, L., Zhao, J., Jiao, Y., Han, T., and Zhou, X. (2024). Improving trans-cleavage activity of CRISPR-Cas13a using engineered crRNA with a uridinylate-rich 5'-overhang. Biosens. Bioelectron. *255*, 116239.

36. Wu, T., Liu, C., Zou, S., Lyu, R., Yang, B., Yan, H., Zhao, M., and Tang, W. (2023). An engineered hypercompact CRISPR-Cas12f system with boosted gene-editing activity. Nat. Chem. Biol. *19*, 1384–1393.

37. Wang, L., Zhou, J., Wang, Q., Wang, Y., and Kang, C. (2021). Rapid design and development of CRISPR-Cas13a targeting SARS-CoV-2 spike protein. Theranostics *11*, 649–664.

38. Gao, Z., Herrera-Carrillo, E., and Berkhout, B. (2018). Delineation of the Exact Transcription Termination Signal for Type 3 Polymerase III. Mol. Ther. Nucleic Acids *10*, 36–44.

39. Bin Moon, S., Lee, J.M., Kang, J.G., Lee, N.-E., Ha, D.-I., Kim, D.Y., Kim, S.H., Yoo, K., Kim, D., Ko, J.-H., and Kim, Y.S. (2018). Highly efficient genome editing by CRISPR-Cpf1 using CRISPR RNA with a uridinylate-rich 3'-overhang. Nat. Commun. *9*, 3651.

40. Rubin, S., Eckhaus, M., Rennick, L.J., Bamford, C.G.G., and Duprex, W.P. (2015). Molecular biology, pathogenesis and pathology of mumps virus. J. Pathol. *235*, 242–252.

41. Wu, H., Wang, F., Tang, D., and Han, D. (2021). Mumps Orchitis: Clinical Aspects and Mechanisms. Front. Immunol. *12*, 582946.

42. Zhao, X., Liu, L., Lang, J., Cheng, K., Wang, Y., Li, X., Shi, J., Wang, Y., and Nie, G. (2018). A CRISPR-Cas13a system for efficient and specific therapeutic targeting of mutant KRAS for pancreatic cancer treatment. Cancer Lett. *431*, 171–181.

43. Ooi, K.H., Liu, M.M., Tay, J.W.D., Teo, S.Y., Kaewsapsak, P., Jin, S., Lee, C.K., Hou, J., Maurer-Stroh, S., Lin, W., et al. (2021). An engineered CRISPR-Cas12a variant and DNA-RNA hybrid guides enable robust and rapid COVID-19 testing. Nat. Commun. *12*, 1739.

44. Liu, Z., Zhang, W., Wang, H., Shangguan, P., Pan, T., Yang, Y., Zhang, Y., Mao, X., Liu, Y., and Zhang, Q. (2024). Engineered CRISPR RNA improves the RNA cleavage efficiency of hfCas13X. FEBS Lett. *598*, 2438–2449.

45. Tamura, K., Stecher, G., and Kumar, S. (2021). MEGA11: Molecular Evolutionary Genetics Analysis Version 11. Mol. Biol. Evol. *38*, 3022–3027.

46. Saitou, N., and Nei, M. (1987). The neighbor-joining method: a new method for reconstructing phylogenetic trees. Mol. Biol. Evol. *4*, 406–425.